RSC Advances

PAPER

View Article Online
View Journal | View Issue



Cite this: *RSC Adv.*, 2023, **13**, 6861

# Optical band gaps and spectroscopy properties of $Bi^{m+}/Eu^{n+}/Yb^{3+}$ co-doped ($m = 0, 2, 3$; and $n = 2, 3$) zinc calcium silicate glasses†

Ho Kim Dan, *[ab] Nguyen Dinh Trung,[cd] Nguyen Minh Tam, [e] L. T. Ha,[f] C. V. Ha, [g] Dacheng Zhou[h] and Jianbei Qiu[h]

Received 18th November 2022
Accepted 2nd February 2023

DOI: 10.1039/d2ra07310b

rsc.li/rsc-advances

In this study, the indirect/direct optical band gaps and spectroscopy properties of $Bi^{m+}/Eu^{n+}/Yb^{3+}$ co-doped ($m = 0, 2, 3$; and $n = 2, 3$) zinc calcium silicate glasses under different excitation wavelengths were investigated. Zinc calcium silicate glasses with the main compositions of $SiO_2$–ZnO–$CaF_2$–$LaF_3$–$TiO_2$ were prepared by the conventional melting method. EDS analysis was performed to determine the elemental composition existing in the zinc calcium silicate glasses. Visible (VIS)-, upconversion (UC)-, and near-infrared (NIR)-emission spectra of $Bi^{m+}/Eu^{n+}/Yb^{3+}$ co-doped glasses were also investigated. Indirect optical band gaps and direct optical band gaps of $Bi^{m+}$-, $Eu^{n+}$- single-doped, and $Bi^{m+}$–$Eu^{n+}$ co-doped $SiO_2$–ZnO–$CaF_2$–$LaF_3$–$TiO_2$–$Bi_2O_3$–$EuF_3$–$YbF_3$ zinc calcium silicate glasses were calculated and analyzed. CIE 1931($x$, $y$) color coordinates for VIS and UC emission spectra of $Bi^{m+}/Eu^{n+}/Yb^{3+}$ co-doped glasses were determined. Besides, the mechanism of VIS-, UC-, NIR-emissions, and energy transfer (ET) processes between $Bi^{m+}$ and $Eu^{n+}$ ions were also proposed and discussed.

## 1. Introduction

During the last several decades, the optical band gaps and spectroscopy properties of host materials single-doped by a rare earth (RE) atom as well as co-doped by rare earth ions (REIs), or doped by REIs together with transition metals (TMs)[1,2] or pnictogen[3] have been extensively studied due to their great potential for applications in many technological fields such as displays, solar cells, and medical diagnosis.[4–6] Among the REIs, europium ions ($Eu^{n+}$) have attracted much research interest, particularly in lighting, light emitting diodes (LED), white LED (WLED), and display applications owing to the $Eu^{n+}$ ions favoring existing in two valence states as the $Eu^{3+}$ trication and $Eu^{2+}$ dication in glass materials with $^5D_0 \rightarrow {}^7F_J$ ($J$=0, 1, 2, 3, and 4) and $4f^65d^1 \rightarrow 4f^7$ transitions, respectively.[7,8] Visible (VIS) emission spectra of $Eu^{3+}/Eu^{2+}$ ions can emit blue, green, orange, orange-red, and red color light depending on the different excitation wavelengths and host materials.[9,10] Bismuth (Bi) element is the post-transition metal belonging to the pnictogen group; Bi exhibits many optoelectronic properties and exists in various valence states such as $Bi^{5+}$, $Bi^{3+}$, $Bi^{2+}$, $Bi^{+}$, and $Bi^0$ depending on the experimental conditions and the host materials. In the VIS wavelength region, the $^1P_1 \rightarrow {}^1S_0$ transition of $Bi^{3+}$ ions can emit blue color light,[11,12] and the $^2S_{1/2}$-, $^2P_{3/2}(2)$-, $^2P_{3/2}(1)$- $\rightarrow {}^2P_{1/2}$ transitions of $Bi^{2+}$ ions can emit orange, orange-red, and red color light, respectively.[12,13] In the near-infrared (NIR) wavelength region, the $^3P_2$-, $^3P_1$- $\rightarrow {}^3P_0$ transitions of $Bi^{+}$ ions and the $^2D_{3/2}$- $\rightarrow {}^4S_{3/2}$ transition of $Bi^0$ neutral can produce NIR emission bands from ~1.0 to 1.35 μm.[14,15] In addition, $Bi^{m+}$ ($m = 0$, 2, and 3) ions can combine with the $^2F_{5/2} \rightarrow {}^2F_{7/2}$ transition of $Yb^{3+}$ ions to generate NIR emission spectra in the ~950 nm to 1350 nm wavelength region.[16,17] Therefore, NIR emission spectra of $Bi^{m+}$–$Yb^{3+}$ have been extensively studied with the aim of improving the efficiency and quantum effect of NIR emission spectra utilized in solar cell applications.[18,19] In recent years, many investigations focusing on the energy transfer (ET) processes from $Bi^{m+}$ to $Eu^{3+}$ ions that can be color-tuned in the VIS emission to create light bands with different colors have been carried out. The obtained results

[a]*Optical Materials Research Group, Science and Technology Advanced Institute, Van Lang University, Ho Chi Minh City, Vietnam*
[b]*Faculty of Applied Technology, School of Technology, Van Lang University, Ho Chi Minh City, Vietnam. E-mail: hokimdan@vlu.edu.vn*
[c]*Center for Analysis and Testing, Dalat University, Lam Dong, Vietnam*
[d]*Faculty of Chemistry and Environment, Dalat University, Lam Dong, Vietnam*
[e]*Faculty of Basic Sciences, University of Phan Thiet, 225 Nguyen Thong, Phan Thiet City, Binh Thuan, Vietnam*
[f]*Institute of Science and Technology, TNU-University of Sciences, Thai Nguyen, 250000, Vietnam*
[g]*Faculty of Physics, TNU-University of Education, Thai Nguyen, 250000, Vietnam*
[h]*Key Laboratory of Advanced Materials of Yunnan Province, School of Materials Science and Engineering, Kunming University of Science and Technology, Kunming 650093, China*

† Electronic supplementary information (ESI) available. See DOI: https://doi.org/10.1039/d2ra07310b

confirmed that the energy was transferred from $Bi^{3+}$ and $Bi^{2+}$ ions to $^5D_0 \rightarrow {}^7F_J$ ($J$=0, 1, 2, 3, and 4) transitions of $Eu^{3+}$ and thus color-tuned the VIS emission spectra of $Eu^{3+}/Eu^{2+}$ ions.[20–23] Besides, the measurement and calculation of the optical band gap parameters of REIs doped in different host materials have also been performed to determine the optical band gap energy ($E_g$) value of REIs in the host materials[24] and thereby directing the relevant optical applications such as color display, LED, WLED, and solar energy. Zinc silicate glasses can be used for optical material applications due to their advantages such as high thermal expansion properties,[26] relatively low glass transition temperature ($T_g$), and the value of $\Delta T = T_c - T_g$ greater than 100.[25] Based on these advantages as well as the results obtained from a recent study,[25] in this work, we chose zinc calcium silicate glass as the host material. In addition, $Na_2O$ was replaced by $CaF_2$ to enhance the self-reduction process from $Eu^{3+}$ to $Eu^{2+}$ ions through $F^-$ ions.[8] Simultaneously, we investigated and reported the results concerning the direct/indirect optical band gaps, VIS-, UC-, and NIR-emission spectra of $Bi^{m+}/Eu^{n+}/Yb^{3+}$ co-doped in $SiO_2$–ZnO–$CaF_2$–$LaF_3$–$TiO_2$ (SZC) zinc calcium silicate glasses. Remarkably, through analyzing the optical properties of $Bi^{m+}/Eu^{n+}/Yb^{3+}$ co-doped, we have also calculated and determined the direct/indirect optical band gaps values, CIE 1931 ($x$, $y$) color coordinates to develop for LED, WLED, and display applications.

## 2. Experimental materials and methods

### 2.1. Materials

Raw materials of $SiO_2$, ZnO, $CaF_2$, $LaF_3$, $TiO_2$, $Bi_2O_3$, $EuF_3$, and $YbF_3$ used in the experiments of this study are high-purity laboratory-grade materials (99.99%). Chemical compositions and ratios for each glass sample are listed in detail in Table 1.

### 2.2. Experimental methods

The raw material mixtures weighing 12 g for each experimental glass sample were crushed with an onyx mortar and pestle.[8,27] These mixtures were compacted into platinum crucibles with lids.[8] The platinum crucibles with lids were then placed in an electric furnace to melt at 1600 °C for 1 hour using the conventional melting method.[8,27] After melting, the mixture was quenched on the surface of the polished stainless steel plate to form the glass.[8] Glass samples were heat treated at 520 °C for 6 hours[8,25] to increase mechanical strength and reduce the possibility of breakage when cut. For the convenience and accuracy of optical measurements, glass samples were cut to the size of 10 mm × 10 mm × 2 mm with polished surfaces and edges.[8] Details for EDS analysis, absorption spectra, VIS-, UC-, and NIR-emission spectra measuring and analyzing devices have been described in detail in our recent studies.[8,27–29]

## 3. Results and discussion

### 3.1. EDS analysis

Fig. 1 shows the results of the EDS spectrum analysis of the SZC-1.0Bi0.6Eu2Yb zinc calcium silicate glass sample. Energy levels at ~0.45 and 4.51 keV were determined for titanium (Ti) element,[30] energy levels at ~2.42 and 10.84 keV were determined for the Bi element, energy levels at ~0.83 and 4.65 keV were attributed to lanthanum (La) element.[30] Energy levels of the Eu element were defined at ~1.13 and 5.85 keV.[30] Energy levels of the ytterbium (Yb) element were also defined at ~1.52 and 7.41 keV. Energy levels at ~0.53, 0.68, 1.74, 3.69, and 8.63 keV were determined for oxygen (O), fluorine (F), silicon (Si), calcium (Ca), and zinc (Zn) elements, respectively.[30,31] The element composition table including weight and atomic percentages of the SZC-1Bi0.6Eu2Yb zinc calcium silicate glass sample inserted in Fig. 1 also described in detail the

Table 1 Chemical compositions and ratios of $SiO_2$–ZnO–$CaF_2$–$LaF_3$–$TiO_2$–$Bi_2O_3$–$EuF_3$–$YbF_3$ glasses

| | Chemical compositions and ratios of glasses (in mol%) | | | | | | | |
|---|---|---|---|---|---|---|---|---|
| Notation of glass samples | $SiO_2$ | ZnO | $CaF_2$ | $LaF_3$ | $TiO_2$ | $Bi_2O_3$ | $EuF_3$ | $YbF_3$ |
| SZC-1Bi | 45 | 25 | 15 | 10 | 4 | 1.0 | 0 | 0 |
| SZC-0.6Eu | 45 | 25 | 15 | 9.4 | 5 | 0 | 0.6 | 0 |
| SZC-1Bi0.6Eu | 45 | 25 | 15 | 9.4 | 4 | 1.0 | 0.6 | 0 |
| SZC-1.8Bi0.6Eu | 45 | 25 | 15 | 9.4 | 3.2 | 1.8 | 0.6 | 0 |
| SZC-1.0Bi0.6Eu2Yb | 45 | 25 | 15 | 7.4 | 4 | 1.0 | 0.6 | 2.0 |
| SZC-1.2Bi0.6Eu2Yb | 45 | 25 | 15 | 7.4 | 3.8 | 1.2 | 0.6 | 2.0 |
| SZC-1.4Bi0.6Eu2Yb | 45 | 25 | 15 | 7.4 | 3.6 | 1.4 | 0.6 | 2.0 |
| SZC-1.6Bi0.6Eu2Yb | 45 | 25 | 15 | 7.4 | 3.4 | 1.6 | 0.6 | 2.0 |
| SZC-1.8Bi0.6Eu2Yb | 45 | 25 | 15 | 7.4 | 3.2 | 1.8 | 0.6 | 2.0 |
| SZC-1.8Bi0.7Eu2Yb | 45 | 25 | 15 | 7.3 | 3.2 | 1.8 | 0.7 | 2.0 |
| SZC-1.8Bi0.8Eu2Yb | 45 | 25 | 15 | 7.2 | 3.2 | 1.8 | 0.8 | 2.0 |
| SZC-1.8Bi0.9Eu2Yb | 45 | 25 | 15 | 7.1 | 3.2 | 1.8 | 0.9 | 2.0 |
| SZC-1.8Bi1.0Eu2Yb | 45 | 25 | 15 | 7 | 3.2 | 1.8 | 1.0 | 2.0 |
| SZC-1.8Bi0.6Eu2.2Yb | 45 | 25 | 15 | 6.8 | 3.2 | 1.8 | 0.6 | 2.2 |
| SZC-1.8Bi0.6Eu2.4Yb | 45 | 25 | 15 | 6.6 | 3.2 | 1.8 | 0.6 | 2.4 |
| SZC-1.8Bi0.6Eu2.6Yb | 45 | 25 | 15 | 6.4 | 3.2 | 1.8 | 0.6 | 2.6 |
| SZC-1.8Bi0.6Eu2.8Yb | 45 | 25 | 15 | 6.2 | 3.2 | 1.8 | 0.6 | 2.8 |

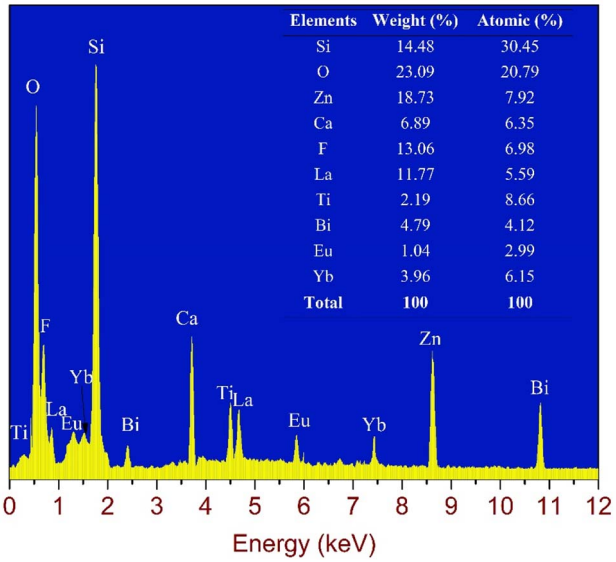


Fig. 1 EDS spectrum of SZC-1.0Bi0.6Eu2Yb zinc calcium silicate glass sample.

proportions of elements present in the host glass. From the results of the EDS analysis, it can be seen that all elements Si, O, Zn, Ca, F, La, Ti, Bi, Eu, and Yb presenting in $SiO_2$–ZnO–$CaF_2$–$LaF_3$–$TiO_2$–$Bi_2O_3$–$EuF_3$–$YbF_3$ raw materials were distributed and existed in zinc calcium silicate glass matrix.

### 3.2. Absorption spectra

Absorption spectra of SZC-1.0Bi, SZC-0.6Eu, and SZC-1.0Bi0.6Eu zinc calcium silicate glass samples in the wavelength range from 300 to 1200 nm are shown in Fig. 2. Curve (*a*) (black curve) in Fig. 2 is the absorption spectrum of $Bi^{m+}$ ions which has three main bands, generated by the transitions of $Bi^{m+}$ ions, with the peaks at ~458, 653, and 700 nm, corresponding to $^1S_0 \rightarrow {}^3P_1$ transition of $Bi^{3+}$ ions,[11,18,29] $^4S_{3/2} \rightarrow {}^2P_{1/2}$ transition of $Bi^0$ ions,[14,15] and $^2P_{1/2} \rightarrow {}^2P_{3/2}(1)$ transition of $Bi^{2+}$ ions.[13] We did not analyze and discuss the absorption spectrum of $Bi^{m+}$ ($m = 0$, 2, and 3) ions in detail in this study. The absorption spectrum of the SZC-0.6Eu zinc calcium silicate glass sample is shown by curve (*b*) (red curve) in Fig. 2. It can be observed that the absorption spectrum of this curve includes four main absorption peaks at ~394, 434, 465, and 536 nm corresponding to transitions from $^7F_0$ ground-state to $^5L_6$, $^5D_3$, $^5D_2$, and $^5D_1$ excited states of $Eu^{3+}$ ions.[7,8,32] The absorption spectrum of the SZC-1.0Bi0.6Eu zinc calcium silicate glass sample is shown by curve (*c*) (blue curve) of Fig. 2. This absorption spectrum includes all the absorption peaks of $Bi^{m+}$ and $Eu^{n+}$ ions present in curves (*a*) and (*b*) due to overlapping and combining absorption spectra of $Bi^{m+}$ and $Eu^{n+}$ ions.[7,8,11,13,32] The images inserted in Fig. 2 are photographs of SZC-1Bi, SZC-0.6Eu, and SZC-1Bi0.6Eu zinc calcium silicate glass samples.

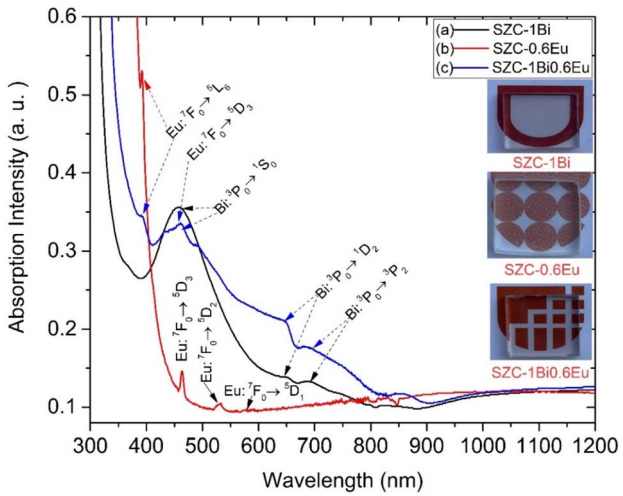


Fig. 2 Absorption spectra of SZC-1.0Bi, SZC-0.6Eu, and SZC-1.0Bi0.6Eu zinc calcium silicate glass samples.

### 3.3. Optical band gaps

Fig. 3 shows the direct optical band gaps (DOBG) (Fig. 3a) and indirect optical band gaps (IOBG) (Fig. 3b) of SZC-1.0Bi, SZC-0.6Eu, and SZC-1.0Bi0.6Eu zinc calcium silicate glass samples. DOBG and IOBG values for SZC-1.0Bi, SZC-0.6Eu, and SZC-1.0Bi0.6Eu zinc calcium silicate glass samples can be calculated based on the absorption spectra of these glass samples, and Tauc following formula:[8]

$$\alpha(\lambda) = A \cdot \frac{(h\nu - E_g)^{\gamma}}{h\nu} \quad (1)$$

In there, $\gamma = 1/2$ for the DOBG, and $\gamma = 2$ for the IOBG; $E_g$ is the energy gap of SZC-1.0Bi, SZC-0.6Eu, and SZC-1.0Bi0.6Eu zinc calcium silicate glass samples; ($\lambda$) is the absorption coefficient; $A$ is a proportionality constant; $\nu$ is the frequency; $h$ is Planck's constant; $\lambda$ is the wavelength. The relation between $\alpha(\lambda)$ and $h\nu$ is given by the Davis and Mott theory.[33] For each glass sample, ($\lambda$) is determined based on the expression:[8,33]

$$\alpha(\lambda) = \frac{2.303}{d} \cdot E_{opt}(\lambda) \quad (2)$$

In there, $E_{opt}(\lambda)$ is the absorbance; $d$ is the thickness of SZC zinc calcium silicate glass samples.[33]

Thus, the DOBG values for SZC-1.0Bi, SZC-0.6Eu, and SZC-1.0Bi0.6Eu zinc calcium silicate glass samples were determined to be ~4.01, 3.47, and 3.96 eV, respectively. Compared with the DOBG value of the SZC-0.6Eu zinc calcium silicate glass sample, the DOBG value of SZC-1.0Bi0.6Eu zinc calcium silicate glass sample was significantly greater with the energy difference $\Delta E_{g(DOBG)} = 3.96\ eV - 3.47\ eV = 0.49\ eV$. The IOBG values for SZC-1.0Bi, SZC-0.6Eu, and SZC-1.0Bi0.6Eu zinc calcium silicate glass samples were determined to be ~3.78, 2.83, and 3.65 eV, respectively. Compared with the IOBG value of the SZC-0.6Eu zinc calcium silicate glass sample, the IOBG value of the SZC-1.0Bi0.6Eu zinc calcium silicate glass sample was also increased significantly with the energy difference $\Delta E_{g(IOBG)} = 3.65\ eV - 2.83\ eV = 0.82\ eV$. This result thus confirmed that both DOBG and IOBG values were significantly increased with the presence of $Bi^{m+}$ ions in the SZC-1.0Bi0.6Eu zinc calcium silicate glass sample. On the contrary, when comparing the

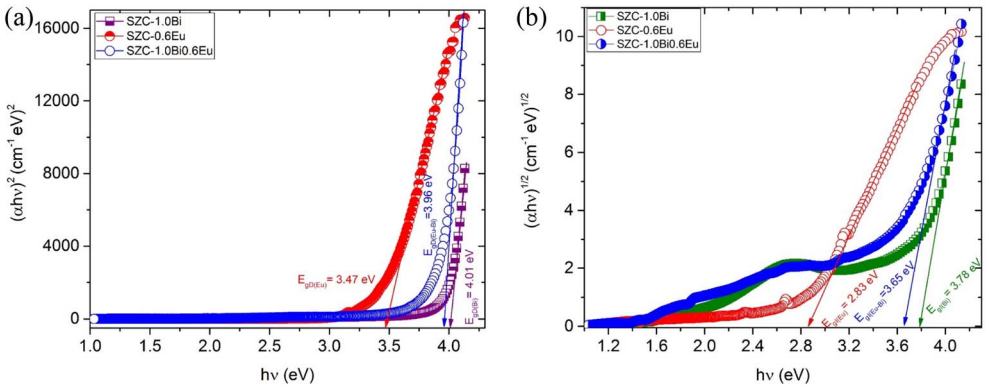


Fig. 3 (a) Direct optical band gaps of SZC-1.0Bi, SZC-0.6Eu, and SZC-1.0Bi0.6Eu zinc calcium silicate glass samples. (b) Indirect optical band gaps of SZC-1.0Bi, SZC-0.6Eu, and SZC-1.0Bi0.6Eu zinc calcium silicate glass samples.

DOBG and IOBG values of the SZC-1Bi sample with the corresponding DOBG and IOBG values of the SZC-1Bi0.6Eu sample, both DOBG and IOBG values of the SZC-1Bi0.6Eu sample are all significantly decreased. These results can be rationalized by the following reasons: (i) the absorption spectrum of the SZC-0.6Eu sample does not appear in the surface plasmon resonance (SPR),[34] whereas for the SZC-1Bi0.6Eu, sample, the absorption spectrum appears in the SPR at the peak of ~458 nm of $Bi^{m+}$ ions. Therefore, the $E_{opt}(\lambda)$ value of the SZC-1Bi0.6Eu sample increases more than the $E_{opt}(\lambda)$ value of the SZC-0.6Eu sample[34] leading to the values of both DOBG and IOBG of the sample SZC-1Bi0.6Eu increase according to formula (1); (ii) compared with the SZC-1Bi sample, the $E_{opt}(\lambda)$ value of the SZC-1Bi0.6Eu sample decreases linearly in the presence of $Eu^{n+}$ ions due to $Eu^{n+}$ ions combining with $Bi^{m+}$ ions to increase the non-bridging oxygen (NBO) bonds[35] leading to the band edge shift to higher energies.[35] The calculated results for DOBG and IOBG values in this work are also completely consistent with the results of previous studies[36–39] and are compared in detail in Table 2. The IOBG value of SZC-1.0Bi, SZC-0.6Eu, and SZC-1.0Bi0.6Eu zinc calcium silicate glass samples showed that the green and blue curves exhibited shallow collisions centered about 2.71 eV. This result is due to both absorption spectra of SZC-1Bi and SZC-1Bi06Eu samples, the peak was at about 458 nm, corresponding to the $h\nu = 2.71$ eV, and thus it appeared the SPR attributed to $Bi^{m+}$ ions.

Table 2 The comparison of direct and indirect optical band gaps in this work with previous related studies[36–39]

| Host materials | Doped/ co-doped | DOBG (eV) | IOBG (eV) | Ref. |
|---|---|---|---|---|
| Germanium-borate glasses | $1.0Bi^{3+}$ | — | 3.43 | X. Y. Liu *et al.*[36] |
| Germanium-borate glasses | $1.0Bi^{3+}$/ $3.5Eu^{3+}$ | — | 3.35 | X. Y. Liu *et al.*[36] |
| Boron glasses | $1Eu^{3+}$ | 3.529 | 3.306 | K. Maheshvaran *et al.*[37] |
| Boro-tellurite glasses | $1Eu^{3+}$ | 3.161 | 3.011 | K. Maheshvaran *et al.*[37] |
| Zinc soda lime silica glasses | $4.7Eu^{3+}$ | 3.20 | — | N. A. S. Omar *et al.*[38] |
| Borosilicate glasses | $10Bi^{3+}$/ $0.6Eu^{3+}$ | 3.430 | 3.419 | D. V. K. Reddy *et al.*[39] |
| Borosilicate glasses | $10Bi^{3+}$/ $1Eu^{3+}$ | 3.456 | 3.449 | D. V. K. Reddy *et al.*[39] |
| Zinc calcium silicate glasses | $0.6Eu^{3+}$ | 3.47 | 2.83 | This study |
| Zinc calcium silicate glasses | $1Bi^{3+}$ | 4.01 | 3.78 | This study |
| Zinc calcium silicate glasses | $1Bi^{3+}$/ $0.6Eu^{3+}$ | 3.96 | 3.65 | This study |

### 3.4. Visible (VIS) emission

Visible (VIS) emission spectra of SZC-1.0Bi, SZC-0.6Eu, SZC-1.0Bi0.6Eu2Yb, and SZC-1.8Bi0.6Eu2Yb zinc calcium silicate glass samples under 320 nm excitation are shown in Fig. 4. For

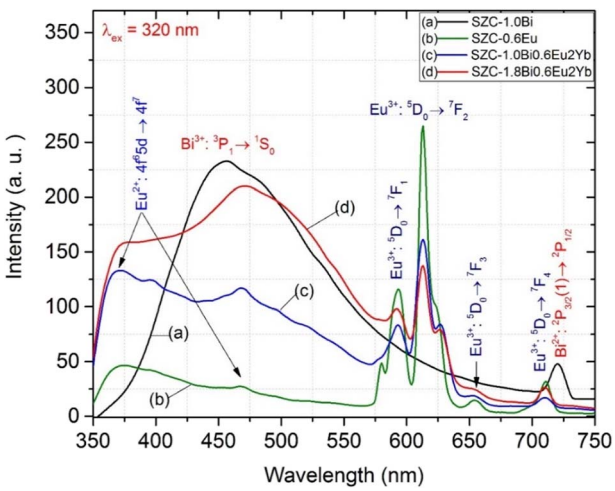


Fig. 4 VIS emission spectra of SZC-1.0Bi, SZC-0.6Eu, SACL-1.0Bi0.6Eu2Yb and SACL-1.8Bi0.6Eu2Yb zinc calcium silicate glass samples under 320 nm excitation.

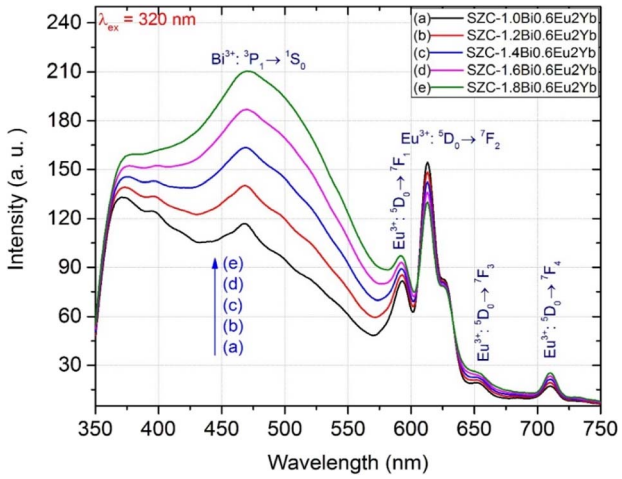


Fig. 5 VIS emission spectra of SZC-*x*Bi0.6Eu2Yb ($x$ = 1.0, 1.2, 1.4, 1.6, and 1.8 mol%) zinc calcium silicate glass samples under 320 nm excitation.

the SZC-1.0Bi zinc calcium silicate glass sample, VIS emission spectra of $Bi^{m+}$ ions were observed consisting of two peaks at ~457 and 720 nm, which are attributed to VIS emissions from $^3P_1 \rightarrow {}^1S_0$ transition of $Bi^{3+}$[11] and $^2P_{3/2}(1) \rightarrow {}^2P_{1/2}$ transition of $Bi^{2+}$,[12,13] respectively. For the SZC-0.6Eu zinc calcium silicate glass sample, VIS emission spectra of $Eu^{3+}/Eu^{2+}$ ions were observed in a band from ~373 to 468 nm, attributed to VIS emission from $4f^65d^1 \rightarrow 4f^7$ transition of $Eu^{2+}$ ions,[7,8] and four VIS emission peaks at ~593, 613, 654, and 710 nm attributed to $^5D_0 \rightarrow {}^7F_J$ ($J$=1, 2, 3, and 4) transitions of $Eu^{3+}$ ions.[20,21] For the SZC-1.0Bi0.6Eu2Yb and SZC-1.8Bi0.6Eu2Yb zinc calcium silicate glass samples, VIS emission intensity of $Eu^{3+}/Eu^{2+}$ ions in the band of 373–468 nm was significantly increased due to ET process from $Bi^{3+}$ to $Eu^{2+}$ ions. The remaining VIS emission spectra of $Eu^{3+}$ ions peaks at ~593, 613, 654, and 710 nm were also observed.[21,22] However, the VIS emission spectra of $Bi^{2+}$ ions peak at ~720 nm have ceased to exist and can not be observed. This result also means that the energy from the $^2P_{3/2}(1) \rightarrow {}^2P_{1/2}$ transition of $Bi^{2+}$ ions is transferred to $^5D_0 \rightarrow {}^7F_4$ neighboring transition of $Eu^{3+}$ ions.[20–22]

VIS emission spectra of SZC-*x*Bi0.6Eu2Yb ($x$ = 1.0, 1.2, 1.4, 1.6, and 1.8 mol%) zinc calcium silicate glass samples under 320 nm excitation are shown in Fig. 5. With the increasing of $Bi^{m+}$ concentrations from 1.0 up to 1.8 mol%, the VIS emission intensity of the peak at ~468 nm was strongly increased. At the same time, the VIS emission intensity of the peaks at ~593, 613, 654, and 710 nm of $Eu^{3+}$ were also increased. This proves that the energy from $^3P_1 \rightarrow {}^1S_0$ transition of $Bi^{3+}$ ions[11,12] and $^2P_{3/2}(1) \rightarrow {}^2P_{1/2}$ transition of $Bi^{2+}$ ions[17,18] is transferred to $^5D_0 \rightarrow {}^7F_J$ ($J$=1, 2, 3, and 4) transitions of $Eu^{3+}$ ions.[7,8,32]

For the $Eu^{3+}/Eu^{2+}$-doped and $Bi^{m+}/Eu^{3+}/Eu^{2+}$ co-doped in the glass materials, the determination of color coordinates is significant for LED, WLED, and color display applications. Therefore, we calculated and determined CIE 1931 ($x$, $y$) color coordinates for these samples using the CIE chromaticity coordinates calculation software. CIE 1931 ($x$, $y$) color coordinates for the VIS emission spectra of SZC-0.6Eu and SZC-*x*Bi0.6Eu2Yb ($x$ = 1.0, 1.2, 1.4, 1.6, and 1.8 mol%) zinc calcium silicate glass samples under 320 nm excitation are described in detail in Fig. 6. For the $Eu^{3+}/Eu^{2+}$-doped in SZC-0.6Eu zinc calcium silicate glass sample, CIE 1931 ($x$, $y$) color coordinates for VIS emission were determined at P0 point in the pink region. For the $Bi^{m+}/Eu^{n+}$ co-doped in SZC-*x*Bi0.6Eu2Yb ($x$ = 1.0, 1.2, 1.4, 1.6, and 1.8 mol%) zinc calcium silicate glass samples, CIE 1931 ($x$, $y$) color coordinates were determined at P1, P2, P3, P4, and P5 points in the white pink region, which is the neighborhood around black body curve. CIE 1931 ($x$, $y$) color coordinates of P0, P1, P2, P3, P4, and P5 points are listed in detail in Table 3.

### 3.5. Upconversion (UC) emission

Fig. 7 shows the UC emission spectra of SZC-1.8Bi*y*Eu2Yb ($y$ = 0.6, 0.7, 0.8, 0.9, and 1.0 mol%) zinc calcium silicate glass samples under 980 nm LD excitation. From the results presented in Fig. 7, we can determine that the UC emission peaks at ~580, 593, 613, 654, and 706 nm, which are attributed to $^5D_0 \rightarrow {}^7F_J$ ($J$=0, 1, 2, 3, and 4) transitions of $Eu^{3+}$ ions.[40] Under 980 nm LD excitation, UC emission of $Bi^{m+}$ ions was hardly observed at any peaks. At the same time, when increasing the $Eu^{3+}/Eu^{2+}$ concentrations from 0.6 up to 1.0 mol%, UC emission intensity of $Eu^{3+}$ peaks at ~580, 593, 613, 654, and 706 nm was significantly increased.[41,42] The mechanism of the UC process of $Bi^{m+}/Eu^{n+}/Yb^{3+}$ co-doped is depicted in Fig. 10. When excited at the wavelength of 980 nm, two $Yb^{3+}$ ions are formed $Yb^{3+}$–$Yb^{3+}$ pairs. Through the CET 1 process, the photons are transferred to the $^5D_2$ level of $Eu^{3+}$. Then the photons rapidly transfer to the $^5D_0$ level *via* the non-radiative transition. The $^5D_0 \rightarrow {}^7F_J$ ($J$ = 4, 3,

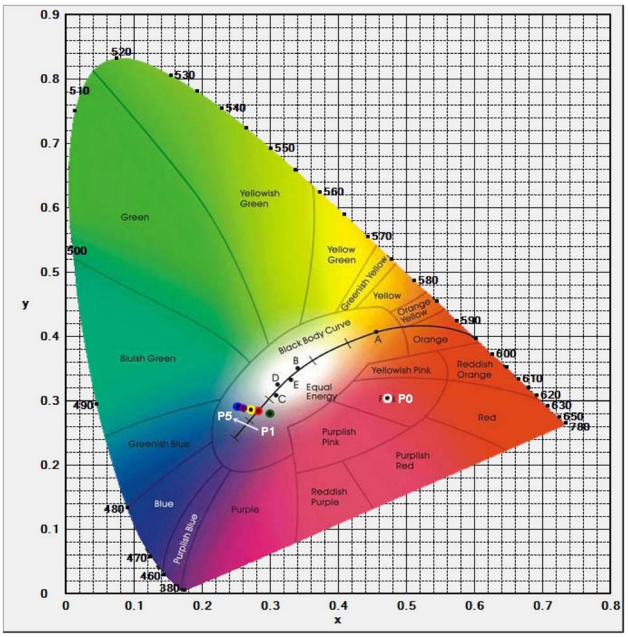


Fig. 6 CIE 1931 ($x$, $y$) color coordinates for VIS emission of SZC-0.6Eu and SZC-*x*Bi0.6Eu2Yb ($x$ = 1.0, 1.2, 1.4, 1.6, and 1.8 mol%) zinc calcium silicate glass samples under 320 nm excitation.

Table 3 CIE 1931 ($x$, $y$) color coordinates of SZC-0.6Eu and SZC-$x$Bi0.6Eu2Yb ($x$ = 1.0, 1.2, 1.4, 1.6, and 1.8 mol%) zinc calcium silicate glass samples under 320 nm excitation

| Glass samples | Position on CIE 1931 chromaticity diagram | CIE 1931 ($x$) | CIE 1931 ($y$) |
|---|---|---|---|
| SZC-0.6Eu | P0 | 0.2534 | 0.2902 |
| SZC-1.0Bi0.6Eu2Yb | P1 | 0.2992 | 0.2801 |
| SZC-1.2Bi0.6Eu2Yb | P2 | 0.2832 | 0.2837 |
| SZC-1.4Bi0.6Eu2Yb | P3 | 0.2710 | 0.2865 |
| SZC-1.6Bi0.6Eu2Yb | P4 | 0.2614 | 0.2886 |
| SZC-1.8Bi0.6Eu2Yb | P5 | 0.2537 | 0.2904 |

2, 1 and 0) transitions of $Eu^{3+}$ produce the UC emissions peaks at ~580, 593, 613, 654, and 706 nm, respectively.

CIE 1931 ($x$, $y$) coordinates for the UC emission spectra of SZC-1.8Bi$y$Eu2Yb ($y$ = 0.6, 0.7, 0.8, 0.9, and 1.0 mol%) zinc calcium silicate glass samples under 980 nm LD excitation is also described in detail in Fig. 8. Based on the results in Fig. 8, it can be seen that the CIE 1931 ($x$, $y$) color coordinates for UC emission spectra of SZC-1.8Bi$y$Eu2Yb ($y$ = 0.6, 0.7, 0.8, 0.9 and 1.0 mol%) zinc calcium silicate glass samples were determined at M1, M2, M3, M4, and M5 points in the reddish-orange region. For the SZC-1.8Bi0.8Eu2Yb, SZC-1.8Bi0.9Eu2Yb, and SZC-1.8Bi1.0Eu2Yb zinc calcium silicate glass samples, although the UC emission intensity at ~580, 593, 613, 654, and 706 nm was significantly increased, but CIE 1931 ($x$, $y$) color coordinates changed very little, the M3, M4, and M5 points almost coincide. CIE 1931 ($x$, $y$) color coordinates of M1, M2, M3, M4, and M5 points are listed in detail in Table 4. Moreover, the comparison of the CIE 1931 ($x$, $y$) color coordinates in this study with those in a few previous related studies[4,36,43–47] is presented in Table 5. From the results revealed in Table 5, we can confirm that with the difference of the host materials, the ratio of $Bi^{3+}/Eu^{3+}$ concentrations, and the excitation wavelength, the CIE 1931 ($x$, $y$) color coordinates also changes differently.

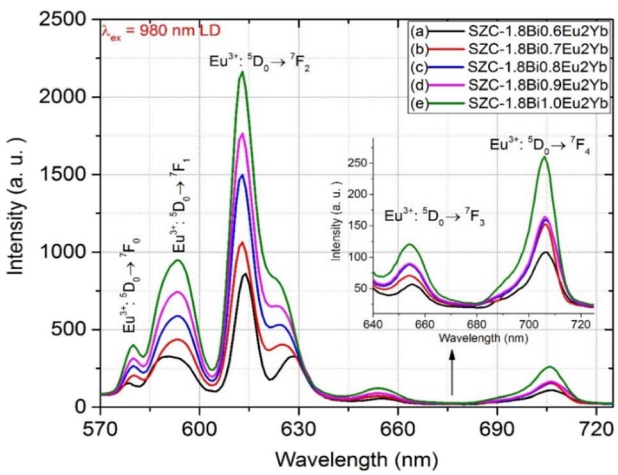


Fig. 7 UC emission spectra of SZC-1.8Bi$y$Eu2Yb ($y$ = 0.6, 0.7, 0.8, 0.9, and 1.0 mol%) zinc calcium silicate glass samples.

### 3.6. NIR emission

NIR emission spectra of SZC-1Bi0.6Eu$z$Yb ($z$ = 2.0, 2.2, 2.4, 2.6, and 2.8 mol%) zinc calcium silicate glass samples under excitation of 330 nm are shown in Fig. 9. It can be observed that the NIR emission spectra of $Bi^{m+}/Eu^{n+}/Yb^{3+}$ co-doped ($m$ = 0, 2, 3 and $n$ = 2, 3) consist of two emission peaks at ~986 and 1062 nm, which the NIR emission of $Bi^{m+}/Eu^{n+}/Yb^{3+}$ co-doped peak at ~986 nm due to $^2F_{5/2} \rightarrow {}^2F_{7/2}$ transition of $Yb^{3+}$ ions,[48] while the NIR emission peak at ~1062 nm can be attributed to $^2D_{3/2} \rightarrow {}^4S_{3/2}$ transition of $Bi^0$ ions.[48–50] In the NIR range of ~960–1040 nm, NIR emission spectra of $Bi^{m+}/Eu^{n+}/Yb^{3+}$ co-doped produced a bandwidth of ~40 nm. However, according to many previous reports, it has been attributed the NIR emission at ~1062 nm to $Bi^0$ ions because Bi-dopant exists at three states including $Bi^{3+}$, $Bi^+$, and $Bi^0$ ions that can emit in NIR range from ~950 to 1500 nm,.[12,15–17] It thus has been confirmed that (i) NIR emission of Bi-doped peak around

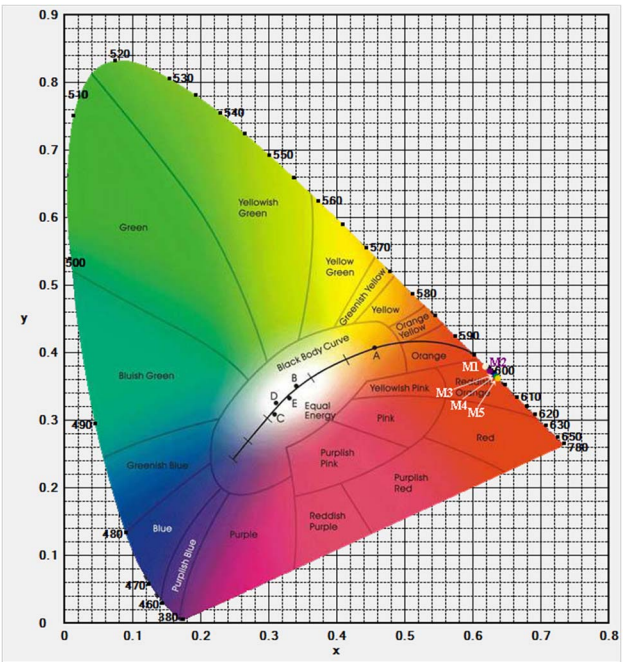


Fig. 8 CIE 1931 ($x$, $y$) for UC emission spectra of SZC-1.8Bi$y$Eu2Yb ($y$ = 0.6, 0.7, 0.8, 0.9, and 1.0 mol%) zinc calcium silicate glass samples under 980 nm LD excitation.

Table 4 CIE 1931 (*x*, *y*) color coordinates of SZC-1.8Bi*y*Eu2Yb (*y* = 0.6, 0.7, 0.8, 0.9, and 1.0 mol%) zinc calcium silicate glass samples under 980 nm LD excitation

| Glass samples | Position on CIE 1931 chromaticity diagram | CIE 1931 (*x*) | CIE 1931 (*y*) |
|---|---|---|---|
| SZC-1.8Bi0.6Eu2Yb | M1 | 0.6239 | 0.3756 |
| SZC-1.8Bi0.7Eu2Yb | M2 | 0.6293 | 0.3703 |
| SZC-1.8Bi0.8Eu2Yb | M3 | 0.6317 | 0.3679 |
| SZC-1.8Bi0.9Eu2Yb | M4 | 0.6321 | 0.3675 |
| SZC-1.8Bi1.0Eu2Yb | M5 | 0.6322 | 0.3674 |

Table 5 The CIE 1931 (*x*, *y*) color coordinates in this work in comparison with those in previous related studies.[4,36,43–47]

| Host materials | Doped/ co-doped | $\lambda_{ex}$ (nm) | CIE 1931(*x*, *y*) | Color region | Ref. |
|---|---|---|---|---|---|
| Germanium-borate glasses | $1.0Bi^{3+}/0.5Eu^{3+}$ | 345 | (0.356, 0.325) | White | X. Y. Liu *et al.*[36] |
| Germanium-borate glasses | $1.0Bi^{3+}/3.5Eu^{3+}$ | 345 | (0.562, 0.371) | Reddish orange | X. Y. Liu *et al.*[36] |
| $Ba_2Y_5B_5O_{17}$ phosphors | $0.0005Bi^{3+}/0.4Eu^{3+}$ | 365 | (0.415, 0.359) | Orange pink | G. Annadurai *et al.*[43] |
| $Lu_2Ge_2O_7$ phosphors | $0.06Bi^{3+}/0.2Eu^{3+}$ | 290 | (0.558, 0.232) | Purplish red | Q. F. Li *et al.*[4] |
| $(Ba, Sr)_3Sc_4O_9$ solid solution compounds | $0.03Bi^{3+}/0.3Eu^{3+}$ | 330 | (0.575, 0.340) | Reddish orange | P. P. Dang *et al.*[44] |
| Silicate glasses | $2Bi^{3+}/0.3Eu^{3+}$ | 333 | (0.595, 0.352) | Reddish orange | O. G. Giraldo *et al.*[45] |
| $KY_3F_{10}$ oxyfluoride glass-ceramics | $0.3Bi^{3+}/0.4Eu^{3+}$ | 280 | (0.2969, 0.2275) | Reddish purple | B. C. Yu *et al.*[46] |
| $LaNbO_4$ phosphor | $0.12Eu^{3+}/0.05Yb^{3+}$ | 980 | (0.560, 0.390) | Orange | A. Dwivedi *et al.*[47] |
| Zinc calcium silicate glasses | $0.6Eu^{3+}$ | 320 | (0.2534, 0.2902) | Pink | This study |
| Zinc calcium silicate glasses | $1Bi^{3+}/0.6Eu^{3+}/2Yb^{3+}$ | 320 | (0.2992, 0.2801) | Purplish blue (near the white area) | This study |
| Zinc calcium silicate glasses | $1.8Bi^{3+}/0.6Eu^{3+}/2Yb^{3+}$ | 980 | (0.6239, 0.3756) | Reddish orange | This study |

1100 nm was attributed to $Bi^0$ ions;[38] (ii) the NIR emission spectrum of $Bi^{3+}$ ions was unobserved in the NIR wavelength range[15–17] and that NIR emission of $Bi^{3+}$ under different excitation wavelengths is usually emitted from ~1250 to 1500 nm.[11,39] With the increase of $Yb^{3+}$ concentrations from 2.0 up to 2.8 mol% and $Bi^{m+}$ concentrations remained unchanged, NIR emission intensity of $Bi^0$ ions peak at ~1062 nm was decreased. This result has confirmed that ET from $^2D_{3/2} \rightarrow {}^4S_{3/2}$ transition of $Bi^0$ ions to $^2F_{5/2} \rightarrow {}^2F_{7/2}$ transition of $Yb^{3+}$ ions has occurred. At the same time, the NIR emission intensity of $Bi^{m+}/Eu^{n+}/Yb^{3+}$ co-doped peak at ~986 nm was strongly increased due to the energy contribution of cooperative ET $(CET)_4$ and $CET_5$ processes from $Eu^{3+}$ and $Eu^{2+}$ ions to $Yb^{3+}$ ions.[40,41]

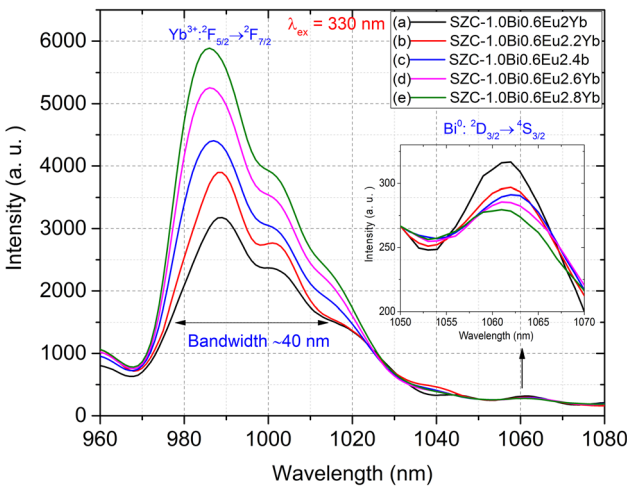


Fig. 9 NIR emission spectra of SZC-1Bi0.6Eu*z*Yb (*z* = 2.0, 2.2, 2.4, 2.6, and 2.8 mol%) zinc calcium silicate glass samples.

Mechanism of $CET_I$ (*I* from 1 to 5) and $ET_J$ (*J* from 1 to 4) processes among $Eu^{n+}$, $Bi^{m+}$, and $Yb^{3+}$ ions in SZC zinc calcium silicate glasses are described and defined in detail in Fig. 10. $CET_I$ (*I* from 1 to 5) and $ET_J$ (*J* from 1 to 4) processes were described as follows:[50–52]

$$CET_1: (^2F_{7/2} + {}^2F_{5/2})(Yb^{3+}) + {}^5D_2(Eu^{3+}) \rightarrow (^2F_{7/2} + {}^2F_{7/2})(Yb^{3+}) + {}^7F_0(Eu^{3+}).$$

$$CET_2: {}^2P_{1/2}(Bi^{3+}) + {}^2F_{7/2}(2Yb^{3+}) \rightarrow {}^1S_0(Bi^{3+}) + {}^2F_{5/2}(2Yb^{3+}).$$

$$CET_3: {}^1S_0(Bi^0) + {}^2F_{7/2}(2Yb^{3+}) \rightarrow {}^4S_{3/2}(Bi^0) + {}^2F_{5/2}(2Yb^{3+}).$$

$$CET_4: {}^5D_2(Eu^{3+}) + {}^2F_{7/2}(2Yb^{3+}) \rightarrow {}^7F_0(Eu^{3+}) + {}^2F_{5/2}(2Yb^{3+}.)$$

$$CET_5: 4f^65d(Eu^{2+}) + {}^2F_{7/2}(2Yb^{3+}) \rightarrow 4f^7(Eu^{2+}) + {}^2F_{5/2}(2Yb^{3+}).$$

$$ET1: 4f^65d(Eu^{2+}) + {}^7F_0(Eu^{3+}) \rightarrow {}^5D_2(Eu^{3+}) + 4f^7(Eu^{2+}).$$

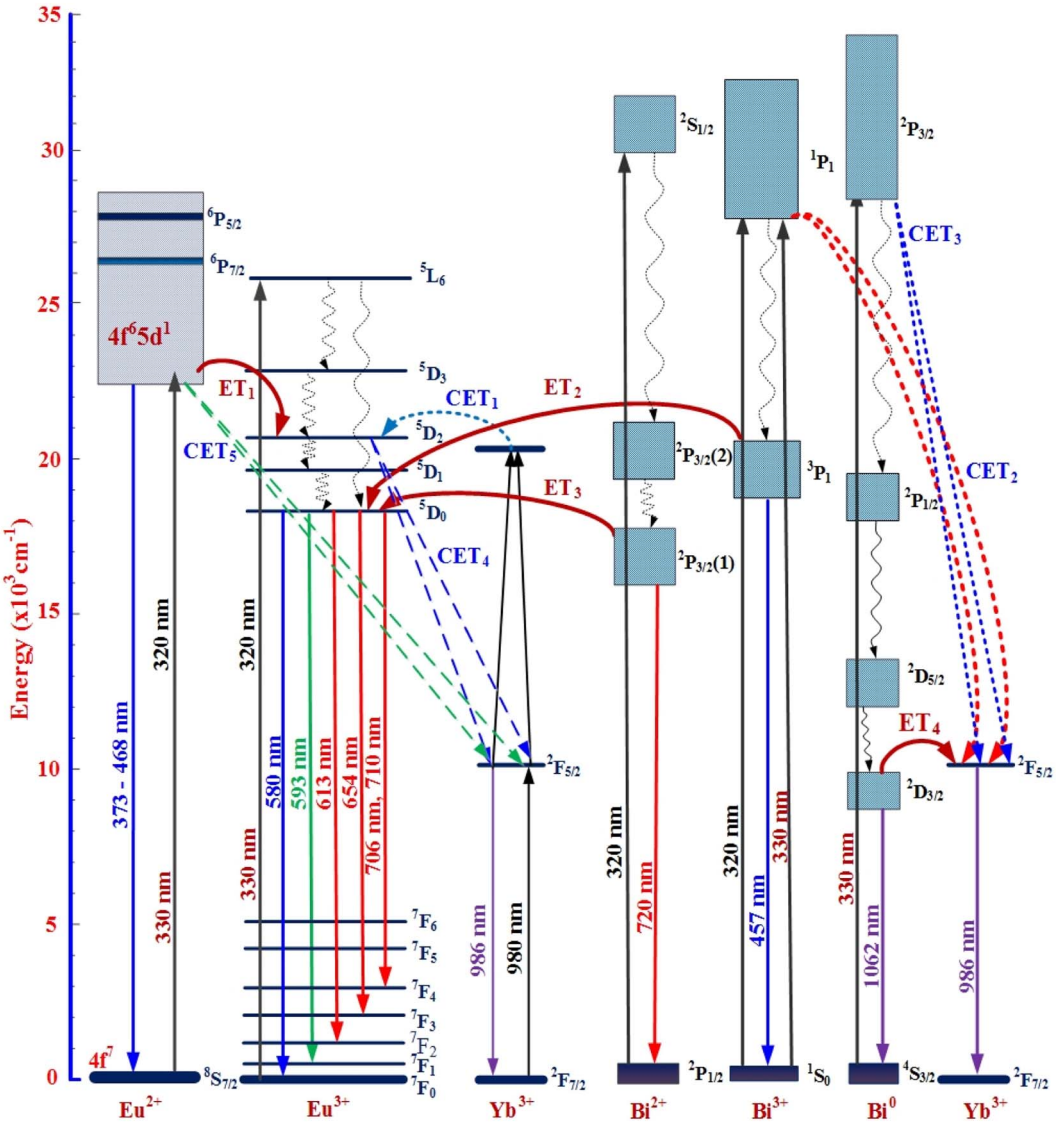


Fig. 10 Energy levels, VIS-, UC-, NIR-emissions and mechanism of CET$_I$ ($I$ from 1 to 5), and ET$_J$ ($J$ from 1 to 4) processes between $Bi^{m+}$, $Eu^{n+}$, and $Yb^{3+}$ in SZC zinc calcium silicate glasses.

ET2: $^3P_1(Bi^{3+}) + {}^7F_0(Eu^{3+}) \rightarrow {}^5D_0(Eu^{3+}) + {}^1S_0(Bi^{3+})$.

ET3: $^2P_{1/2}(1)(Bi^{2+}) + {}^7F_0(Eu^{3+}) \rightarrow {}^5D_0(Eu^{3+}) + {}^2P_{1/2}(Bi^{2+})$.

ET4: $^2D_{3/2}(Bi^0) + {}^2F_{7/2}(Yb^{3+}) \rightarrow {}^2F_{5/2}(Yb^{3+}) + {}^4S_{3/2}(Bi^0)$.

## 4. Conclusions

In this work, we have successfully synthesized zinc calcium silicate glass with the main compositions of $SiO_2$–ZnO–$CaF_2$–$LaF_3$–$TiO_2$–$Bi_2O_3$–$EuF_3$–$YbF_3$. The DOBG and IOBG values for $Bi^{m+}/Eu^{n+}$ co-doped in SZC-1.0Bi0.6Eu zinc calcium silicate glass samples were determined at ~3.65 and 3.96 eV, respectively. Both of these values were increased in the presence of $Bi^{m+}$ ions in SZC-1.0Bi0.6Eu zinc calcium silicate glass samples. Under the excitation of 320 nm, VIS emission spectra of $Bi^{m+}/Eu^{n+}/Yb^{3+}$ co-doped were observed in the peaks at ~468, 593, 613, 654, and 710 nm attributed to $Bi^{3+}$, $Bi^{2+}$, $Eu^{3+}$, and $Eu^{2+}$ ions. CIE 1931 ($x$, $y$) color coordinates for VIS emission spectra of $Bi^{m+}/Eu^{n+}/Yb^{3+}$ co-doped zinc calcium silicate glass samples were determined in the white-pink region neighborhood around the black body curve. UC emission spectra of $Bi^{m+}/Eu^{n+}/Yb^{3+}$ co-doped were observed in the peaks at ~580, 593, 613, 654, and 706 nm attributed to $Eu^{2+}$ ions. CIE 1931 ($x$, $y$) color coordinates for UC emission spectra of $Bi^{m+}/Eu^{n+}/Yb^{3+}$ co-doped zinc calcium silicate glass samples were determined in the reddish-orange region. NIR emission spectra of $Bi^{m+}/Eu^{n+}/Yb^{3+}$ co-doped have two emission peaks at ~986 and 1062 nm, attributed to $Yb^{3+}$ and $Bi^0$ ions, respectively. NIR emission

spectra of $Bi^{m+}/Eu^{n+}/Yb^{3+}$ co-doped produced a bandwidth of ~40 nm in the wavelength range of ~960 to 1040 nm. The energy from $^3P_1 \rightarrow {}^1S_0$ transition of $Bi^{3+}$ ions and $^2P_{3/2}(1) \rightarrow {}^2P_{1/2}$ transition of $Bi^{2+}$ ions transferred to $^5D_0 \rightarrow {}^7F_J$ ($J$=1, 2, 3, and 4) transitions of $Eu^{3+}$ ions and ET process from $^2D_{3/2} \rightarrow {}^4S_{3/2}$ transition of $Bi^0$ ions to $^2F_{5/2} \rightarrow {}^2F_{7/2}$ transition of $Yb^{3+}$ ions also occurred. The $Bi^{m+}/Eu^{n+}/Yb^{3+}$ co-doped zinc calcium silicate glasses in this study can be further developed for LED, WLED, display, and solar cell applications.

## Conflicts of interest

There are no conflicts to declare.

## Acknowledgements

This research is funded by Projects B2022-TNA-37 of the Vietnam Ministry of Education and Training. The author Ho Kim Dan would like to express his gratitude to Van Lang University.

## References

1 A. D. Sontakke, A. J. van Bunningen, F. T. Rabouw, S. Meijers and A. Meijerink, Unraveling the $Eu^{2+} \rightarrow Mn^{2+}$ energy transfer mechanism in W-LED phosphors, *J. Phys. Chem. C*, 2020, **124**(25), 13902–13911, DOI: 10.1021/acs.jpcc.0c03425.

2 H. K. Dan, D. C. Zhou, R. F. Wang, Q. Jiao, Z. W. Yang, Z. G. Song, X. Yu and J. B. Qiu, Effect of $Mn^{2+}$ ions on the enhancement red upconversion emission and energy transfer of $Mn^{2+}/Tm^{3+}/Yb^{3+}$ tri-doped transparent glass-ceramics, *Mater. Res. Bull.*, 2016, **73**, 357–361, DOI: 10.1016/j.materresbull.2015.09.019.

3 X. Yu, L. Zhang, X. H. Xu, T. Wang, H. L. Yu, T. M. Jiang, Q. Jiao, Z. W. Yang, D. C. Zhou and J. B. Qiu, Development of a single-phased $Ca_3SnSi_2O_9$: $Bi^{3+}$, $Dy^{3+}$, $Eu^{3+}$ phosphor with tri-colors for white light-emitting diodes, *J. Lumin.*, 2014, **145**, 114–118, DOI: 10.1016/j.jlumin.2013.07.009.

4 Q. F. Li, S. A. Zhang, W. X. Lin, W. F. Li, Y. X. Li, Z. F. Mu and F. G. Wu, A warm white emission of $Bi^{3+}$-$Eu^{3+}$ and $Bi^{3+}$-$Sm^{3+}$ codoping $Lu_2Ge_2O_7$ phosphors by energy transfer of $Bi^{3+}$-sensitized $Eu^{3+}/Sm^{3+}$, *Spectrochim. Acta, Part A*, 2020, **228**(5), 117755, DOI: 10.1016/j.saa.2019.117755.

5 Y. Zhydachevskyy, I. I. Syvorotkac, V. Tsiumraa, M. Barand, L. Lipińskad, A. Wierzbickaa and A. Suchocki, Quantum efficiency of the down-conversion process in $Bi^{3+}$-$Yb^{3+}$ and $Ce^{3+}$-$Yb^{3+}$ co-doped garnets, *Sol. Energy Mater. Sol. Cells*, 2018, **185**, 240–251, DOI: 10.1016/j.solmat.2018.05.037.

6 X. Liu, C. Chen, S. Li, Y. Dai, H. Guo, X. Tang, Y. Xie and L. Yan, Host-sensitized and tunable luminescence of $GdNbO_4$:$Ln^{3+}$ ($Ln^{3+}$ = $Eu^{3+}/Tb^{3+}/Tm^{3+}$) nanocrystalline phosphors with abundant color, *Inorg. Chem.*, 2016, **55**, 10383–10396, DOI: 10.1021/acs.inorgchem.6b01637.

7 Y. D. Ma, M. Z. Fei, W. N. Zhang, L. M. Teng, F. F. Hu, R. F. Wei and H. Guo, Energy transfer and tunable luminescent properties in $Eu^{2+}/Tb^{3+}/Eu^{3+}$ co-doped oxyfluoride aluminosilicate glass, *J. Lumin.*, 2020, **219**, 116966, DOI: 10.1016/j.jlumin.2019.116966.

8 H. K. Dan, N. D. Trung, T. H. Le, N. L. Thai, N. M. Ty, D. C. Zhou and J. B. Qiu, Influence of $F^-$ on the reduction process of $Eu^{3+}$ to $Eu^{2+}$ and optical properties of $Eu^{3+}/Eu^{2+}$–$Er^{3+}$–$Yb^{3+}$ co-doped niobate silicate glasses, *J. Non-Cryst. Solids*, 2022, **581**, 121417, DOI: 10.1016/j.jnoncrysol.2022.121417.

9 W. P. Chen, Y. J. Ouyang, M. Mo, H. Z. Zhang and Q. Su, Observation of energy transfer from $Eu^{2+}$ to $Eu^{3+}$ and tunable luminescence in phosphors $YF_3$:Eu prepared by hydrothermal method, *J. Lumin.*, 2021, **229**, 117672, DOI: 10.1016/j.jlumin.2020.117672.

10 H. Bouchouicha, G. Panczer, D. de Ligny, Y. Guyot, M. L. Baesso, L. H. C. Andrade, S. M. Lima and R. Ternane, Synthesis and luminescent properties of $Eu^{3+}/Eu^{2+}$ co-doped calcium aluminosilicate glass - ceramics, *J. Lumin.*, 2016, **169**, 528–533, DOI: 10.1016/j.jlumin.2014.11.054.

11 Q. S. Wu, Y. Y. Li, Y. J. Wang, H. Liu, S. S. Ye, L. Zhao, J. Y. Ding and J. C. Zhou, A novel narrow-band blue-emitting phosphor of $Bi^{3+}$-activated $Sr_3Lu_2Ge_3O_{12}$ based on a highly symmetrical crystal structure used for WLEDs and FEDs, *Chem. Eng. J.*, 2020, **401**, 126130, DOI: 10.1016/j.cej.2020.126130, https://www.sciencedirect.com/journal/chemical-engineering-journal/vol/401/suppl/C1.

12 M. Puchalska, P. Bolek, K. Kot and E. Zych, Luminescence of $Bi^{3+}$ and $Bi^{2+}$ ions in novel Bi-doped $SrAl_4O_7$ phosphor, *Opt. Mater.*, 2020, **107**, 109999, DOI: 10.1016/j.optmat.2020.109999.

13 R. P. Cao, M. Y. Peng and J. R. Qiu, Photoluminescence of $Bi^{2+}$-doped $BaSO_4$ as a red phosphor for white LEDs, *Opt. Express*, 2012, **20**(S6), A977–A983, DOI: 10.1364/OE.20.00A977.

14 N. Zhang, K. N. Sharafudeen, G. P. Dong, M. Y. Peng and J. R. Qiu, Mixed network effect of broadband near-infrared emission in Bi-Doped $B_2O_3$-$GeO_2$ glasses, *J. Am. Ceram. Soc.*, 2012, **95**(12), 3842–3846, DOI: 10.1111/jace.12016.

15 R. F. Wang, J. Liu and Z. Zhang, Luminescence and energy transfer progress in Bi-Yb co-doped germanate glass, *J. Alloys Compd.*, 2016, **688**, 332–336, DOI: 10.1016/j.jallcom.2016.07.152.

16 Y. P. Tai, B. L. Pan, X. G. Du, H. Y. Liu, R. Q. Niu and X. Z. Li, Broadband downconversion in $Bi^{3+}$-$Yb^{3+}$-codoped transparent glass ceramics containing $LaF_3$ nanocrystals, *J. Mater. Sci.: Mater. Electron.*, 2020, **31**, 5117–5123, DOI: 10.1007/s10854-020-03072-9.

17 A. J. Huang, Z. W. Yang, C. Y. Yu, Z. Z. Chai, J. B. Qiu and Z. G. Song, Near-infrared quantum cutting luminescence and energy transfer mechanism of $Ba_2Y(BO_3)_2Cl$: $Bi^{3+}$, $Yb^{3+}$ phosphors, *IEEE Photonics J.*, 2018, **10**, 8400307, DOI: 10.1109/JPHOT.2017.2782842.

18 L.-T. Lin, J.-Q. Chen, C. Deng, L. Tang, D.-J. Chen, J.-X. Meng and L.-W. Cao, Broadband near-infrared quantum-cutting by cooperative energy transfer in $Yb^{3+}$–$Bi^{3+}$ co-doped $CaTiO_3$ for solar cells, *J. Alloys Compd.*, 2015, **640**, 280–284, DOI: 10.1016/j.jallcom.2015.04.031.

19 E. Lee, R. E. Kroon, J. J. Terblans and H. C. Swart, Luminescence properties of $Y_2O_3$: $Bi^{3+}$, $Yb^{3+}$ co-doped

phosphor for application in solar cells, *Phys. B*, 2018, **535**(15), 102–105, DOI: 10.1016/j.physb.2017.06.072.

20 R. P. Cao, Z. Y. Huang, B. Lan, L. Li, X. H. Yi, Z. Y. Luo, C. X. Liao and J. Wang, Adjustable luminescence properties of $Eu^{3+}$ and $Bi^{3+}$ codoped $Ca_3Zn_3Te_2O_{12}$ phosphor, *Mater. Res. Bull.*, 2022, **152**, 111851, DOI: 10.1016/j.materresbull.2022.111851, https://www.sciencedirect.com/journal/materials-research-bulletin/vol/152/suppl/C.

21 H. Zhang, M. S. Liao, Y. Jiao, W. C. Li, H. H. Dong, Y. Z. Fang, W. Q. Gao and L. L. Hu, Color-tunable emissions in $Bi^{3+}/Eu^{3+}$ activated phosphors for multi-mode optical thermometers, *Ceram. Interfaces*, 2022, **48**(22), 33072–33081, DOI: 10.1016/j.ceramint.2022.07.240, https://www.sciencedirect.com/journal/ceramics-international/vol/48/issue/22.

22 L. D. Guo, T. Li, C. C. Zhu, W. C. Liang and L. N. Wu, Tunable luminescent chromaticity of CaZnOS: $Bi^{3+}$, $Eu^{3+}$ with white emitting based on energy transfer, *J. Alloys Compd.*, 2022, **905**, 164262, DOI: 10.1016/j.jallcom.2022.164262.

23 Z. Tang, J. Q. Qi, Z. Y. Huang, L. X. Liang, A. J. Liu, Y. C. Ye, Y. T. Zhang and T. C. Lu, Novel multicolor-tunable $Eu^{3+}/Bi^{3+}$ co-doped $Y_2Zr_2O_7$ transparent ceramics as potential white-light-emitting materials, *Ceram. Interfaces*, 2022, **48**(3), 4216–4222, DOI: 10.1016/j.ceramint.2021.10.213, https://www.sciencedirect.com/journal/ceramics-international/vol/48/issue/22.

24 E. Erol, N. Vahedigharehchopogh, O. Kıbrıslı, M. C. Ersundu and A. E. Ersundu, Recent progress in lanthanide-doped luminescent glasses for solid-state lighting applications - a review, *J. Phys.: Condens. Matter*, 2021, **33**, 483001, DOI: 10.1088/1361-648X/ac22d9.

25 H. K. Dan, N. M. Ty, D. C. Zhou, J. B. Qiu and A.-. L. Phan, Influence of $Cr^{3+}$ on yellowish-green UC emission and energy transfer of $Er^{3+}/Cr^{3+}/Yb^{3+}$ tri-doped zinc silicate glasses, *J. Am. Ceram. Soc.*, 2020, **103**(11), 1–13, DOI: 10.1111/jace.17359.

26 D. Ehrt and S. Flügel, Properties of zinc silicate glasses and melts, *J. Mater. Sci. Eng.*, 2011, **A 1**, 312–320.

27 H. K. Dan, D. C. Zhou, R. F. Wang, Q. Jiao, Z. W. Yang, Z. G. Song, X. Yu and J. B. Qiu, Effect of $Mn^{2+}$ ions on the enhancement upconversion emission and energy transfer of $Mn^{2+}/Tb^{3+}/Yb^{3+}$ tri-doped transparent glass-ceramics, *Mater. Lett.*, 2015, **150**, 76–80, DOI: 10.1016/j.matlet.2015.03.005.

28 H. K. Dan, A.-. L. Phan, N. M. Ty, D. C. Zhou and J. B. Qiu, Optical bandgaps and visible/near-infrared emissions of $Bi^{n+}$-doped ($n$ = 1, 2, and 3) fluoroaluminosilicate glasses *via* $Ag^{+}$-$K^{+}$ ions exchange process, *Opt. Mater.*, 2021, **112**, 110762, DOI: 10.1016/j.optmat.2020.110762.

29 H. K. Dan, T. D. Tap, H. Nguyen-Truong, N. M. Ty, D. C. Zhou and J. B. Qiu, Effects of heat treatment and $Yb^{3+}$ concentration on the downconversion emission of $Er^{3+}/Yb^{3+}$ co-doped transparent silicate glass-ceramics, *Mater. Res.*, 2019, **22**(5), e20190113, DOI: 10.1590/1980-5373-MR-2019-0113.

30 Y. G. Liao, *X-Ray emission lines & Periodic table for EDS Analysis, Practical Electron Microscopy and Database - An Online Book*, https://www.globalsino.com/EM, accessed 15 November 2022.

31 N. W. M. Ritchie, D. E. Newbury, H. Lowers and M. Mengason, Exploring the limits of EDS microanalysis: rare earth element analyses, *IOP Conf. Ser.: Mater. Sci. Eng.*, 2018, **304**, 012013, DOI: 10.1088/1757-899X/304/1/012013.

32 K. Lenczewska, Y. Gerasymchuk, N. Vu, N. Q. Liem, G. Boulon and D. Hreniak, The size effect on the energy transfer in $Bi^{3+}$–$Eu^{3+}$ co-doped $GdVO_4$ nanocrystals, *J. Mater. Chem. C*, 2017, **5**, 3014–3023, DOI: 10.1039/C6TC04660F.

33 N. F. Mott and E. A. Davis, *Electronic processes in Non-crystalline materials*, Oxford, UK, Clarendon, 2nd edn, 1979.

34 S. P. Singh and B. Karmakar, Photoluminescence enhancement of $Eu^{3+}$ by energy transfer from $Bi^{2+}$ to $Eu^{3+}$ in bismuth glass nanocomposites, *RSC Adv.*, 2011, **1**, 751–754, DOI: 10.1039/C1RA00160D.

35 M. H. M. Zaid, K. A. Matori, S. H. A. Aziz, A. Zakaria and M. S. M. Ghazali, Effect of ZnO on the physical properties and optical band gap of soda lime silicate glass, *Int. J. Mol. Sci.*, 2012, **13**, 7550–7558, DOI: 10.3390/ijms13067550.

36 X. Y. Liu, H. Guo, S. X. Dai, M. Y. Peng and Q. Y. Zhang, Energy transfer and thermal stability in $Bi^{3+}/Eu^{3+}$ co-doped germanium-borate glasses for organic-resin-free UV LEDs, *Opt. Mater. Express*, 2016, **6**(11), 3574, DOI: 10.1364/OME.6.003574.

37 K. Maheshvaran, P. K. Veeran and K. Marimuthu, Structural and optical studies on $Eu^{3+}$ doped boro-tellurite glasses, *Solid State Sci.*, 2013, **17**, 54–62, DOI: 10.1016/j.solidstatesciences.2012.11.013.

38 N. A. S. Omar, Y. W. Fen, K. A. Matori, M. H. M. Zaid and N. F. Samsudin, Structural and optical properties of $Eu^{3+}$ activated low cost zinc soda lime silica glasses, *Results Phys.*, 2016, **6**, 640–644, DOI: 10.1016/j.rinp.2016.09.007.

39 D. V. K. Reddy, S. Taherunnisa, A. L. Prasanna, T. S. Rao, N. Veeraiah and M. R. Reddy, Enhancement of the red emission of $Eu^{3+}$ by $Bi^{3+}$ sensitizers in yttrium alumino bismuth borosilicate glasses, *J. Mol. Struct.*, 2019, **1176**(15), 133–148, DOI: 10.1016/j.molstruc.2018.08.057.

40 A. Dwivedi, K. Mishra and S. B. Rai, Investigation of upconversion, downshifting and quantum–cutting behavior of $Eu^{3+}$, $Yb^{3+}$, $Bi^{3+}$ co-doped $LaNbO_4$ phosphor as a spectral conversion material, *Methods Appl. Fluoresc.*, 2018, **6**, 035001, DOI: 10.1088/2050-6120/aab253.

41 X. X. Han, E. H. Song, W. B. Chen, Y. Y. Zhou and Q. Y. Zhang, Color-tunable upconversion luminescence and prolonged $Eu^{3+}$ fluorescence lifetime in fluoride $KCdF_3$:$Yb^{3+}$, $Mn^{2+}$, $Eu^{3+}$ *via* controllable and efficient energy transfer, *J. Mater. Chem. C*, 2020, **8**, 9836–9844, DOI: 10.1039/D0TC01502D.

42 J. F. Li, Y. Long, Q. C. Zhao, S. P. Zheng, Z. J. Fang and B.-U. Guan, Efficient white upconversion luminescence in $Yb^{3+}/Eu^{3+}$ doubly-doped transparent glass ceramic, *Opt. Express*, 2021, **29**(14), 21763, DOI: 10.1364/OE.431959.

43 G. Annadurai, L. L. Sun, H. Guo and X. Y. Huang, Bright tunable white-light emissions from $Bi^{3+}/Eu^{3+}$ co-doped $Ba_2Y_5B_5O_{17}$ phosphors *via* energy transfer for UV-excited

white light-emitting diodes, *J. Lumin.*, 2020, **226**, 117474, DOI: **10.1016/j.jlumin.2020.117474**.

44 P. P. Dang, S. S. Liang, G. G. Li, H. Z. Lian, M. M. Shang and J. Lin, Broad color tuning of $Bi^{3+}/Eu^{3+}$-doped $(Ba, Sr)_3Sc_4O_9$ solid solution compounds *via* crystal field modulation and energy transfer, *J. Mater. Chem. C*, 2018, **6**, 9990, DOI: **10.1039/C8TC03334J**.

45 O. G. Giraldo, M. Z. Fei, R. F. Wei, L. M. Teng, Z. G. Zheng and H. Guo, Energy transfer and white luminescence in $Bi^{3+}/Eu^{3+}$ co-doped oxide glasses, *J. Lumin.*, 2020, **219**, 116918, DOI: **10.1016/j.jlumin.2019.116918**.

46 B. C. Yu, X. Zhou, H. P. Xia, B. J. Chen and H. W. Song, Novel $Bi^{3+}/Eu^{3+}$ co-doped oxyfluoride transparent $KY_3F_{10}$ glass ceramics with wide tunable emission and high optical temperature sensitivity, *J. Lumin.*, 2021, **239**, 118366, DOI: **10.1016/j.jlumin.2021.118366**.

47 A. Dwivedi, K. Mishra and S. B. Rai, Investigation of Upconversion, downshifting and quantum –cutting behavior of $Eu^{3+}$, $Yb^{3+}$, $Bi^{3+}$ co-doped $LaNbO_4$ phosphor as a spectral conversion material, *Methods Appl. Fluoresc.*, 2018, **6**, 035001, DOI: **10.1088/2050-6120/aab253**.

48 M. Peng, B. Sprenger, M. A. Schmidt, H. G. L. Schwefel and L. Wondraczek, Broadband NIR photoluminescence from Bi-doped $Ba_2P_2O_7$ crystals: Insights into the nature of NIR-emitting Bismuth centers, *Opt. Express*, 2010, **18**, 12852–12863, DOI: **10.1364/OE.18.012852**.

49 J. D. Wu, D. P. Chen, X. K. Wu and J. R. Qiu, Ultra-broad near-infrared emission of Bi-doped $SiO_2$-$Al_2O_3$-$GeO_2$ optical fibers, Chine, *Opt. Lett.*, 2011, **9**(7), 071601, DOI: **10.3788/COL201109.071601**.

50 F. G. Chen, Y. F. Wang, W. W. Chen, P. X. Xiong, B. F. Jiang, S. F. Zhou, Z. J. Ma and M. Y. Peng, Regulating the Bi NIR luminescence behaviours in fluorine and nitrogen co-doped germanate glasses, *Mater. Adv.*, 2021, **2**, 4743–4751, DOI: **10.1039/D1MA00395J**.

51 M.-H. Qu, R.-Z. Wang, Y. Zhang, K.-Y. Li and H. Yan, High efficient antireflective down-conversion $Y_2O_3$: Bi, Yb films with pyramid preferred oriented nano-structure, *J. Appl. Phys.*, 2012, **111**, 093108, DOI: **10.1063/1.4712461**.

52 Y. P. Tai, G. J. Zheng, H. Wang and J. T. Bai, Broadband down-conversion based near-infrared quantum cutting in $Eu^{2+}$–$Yb^{3+}$ co-doped $SrAl_2O_4$ for crystalline silicon solar cells, *J. Solid State Chem.*, 2015, **226**, 250–254, DOI: **10.1016/j.jssc.2015.02.020**.